***Hexa-Wankel*:**

A Geometric and Thermodynamic Hypothesis
for a Six-Apex Rotary Engine with Dual-Zone Sequential Combustion

---

Jimmy Y. Mahardhika
ORCID: 0009-0001-2138-8206

Conceptual paper. This document is not a prototype claim, not a final patent claim, and not a manufacturing specification. Performance claims are presented as design-threshold conditions that must be verified through CAD, CFD, FEA, seal-tribology testing, and dynamometer testing.

Abstract

This paper formulates the *Hexa-Wankel* as a theoretical design hypothesis for a six-apex rotary engine intended to preserve Wankel-like compactness while improving the determinacy of thermal and sealing conditions. The proposed architecture is not a flat hexagonal housing and not two triangular Wankel engines mechanically joined together. It is defined as a single convex six-apex rotor operating within a Wankel-like five-lobe baseline housing, with two housing-fixed combustion regions arranged as dual-zone sequential combustion. The intuitive process is therefore $(1, 2, 3) + (4, 5, 6)$: intake, compression–ignition–expansion, exhaust, followed by a second intake, compression–ignition–expansion, exhaust sequence. The total fuel energy is not doubled, but divided into two pulses, $Q_R + Q_L = Q_{pair}$ with $Q_R \simeq Q_L \simeq Q_{pair}/2$.

The paper derives the kinematic closure for an N-apex rotor, the six-apex/five-lobe gear law, the envelope regularity condition, swept-volume scaling, friction and leakage thresholds, Fourier thermal-harmonic balancing, the torque-kernel condition $K_i(\theta_s) = \mathrm{d}V_i/\,\mathrm{d}\theta_s > 0$, and gas-exchange constraints. It then reports a first-order two-dimensional kinematic validation: numerical chamber-volume computation gives $V_d = 35.786\,\mathrm{cc}$ per chamber in the baseline model, while an added clearance volume of $3.714\,\mathrm{cc}$ represents a target compression ratio near $r = 10.5$. A subsequent torque-kernel validation identifies positive-expansion windows in the right and left combustion zones. Finally, an idealised zero-dimensional indicated-work model using unsmoothed clearance-corrected chamber volume, finite-duration Wiebe heat release, and $W = \int p\,\mathrm{d}V$ yields positive indicated work for the dual-pulse pair: $W_H = 120.05\,\mathrm{J}$, ideal indicated efficiency 53.18%, $p_{max} = 81.14\,\mathrm{bar}$, and $IMEP = 20.23\,\mathrm{bar}$ under the stated no-wall-loss assumptions. A fair equivalent-displacement single-pulse control gives essentially the same ideal work and pressure, while the dual-pulse phase model reduces the theoretical torque-ripple index from 4.02 to 2.74. The strongest supported claim is therefore not guaranteed brake-efficiency superiority, but positive indicated work with redistributed torque loading and a more periodic thermal-sealing environment. The concept remains falsifiable and incomplete until conjugate 3D geometry, port timing, wall heat transfer, CFD, FEA, seal dynamics, and dynamometer validation are performed.

Keywords: Wankel engine; rotary engine; apex seal; phased combustion; thermal harmonics; five-lobe housing; effective displacement; torque kernel; sequential cycle; indicated work; threshold theory.

1 Introduction

The classical Wankel engine possesses mechanical advantages that are difficult for piston engines to reproduce: compactness, low vibration, few reciprocating components, and high power density. In a conventional Wankel engine, a three-apex rotor forms three working chambers inside an epitrochoidal housing; the eccentric shaft rotates three times for one material revolution of the rotor, so that one rotor produces one power event per shaft revolution in an effective four-stroke cycle [5]. This compactness makes the Wankel engine attractive for small vehicles, range extenders, drones, and other applications in which power-to-weight ratio is important.

The weaknesses of the Wankel engine, however, are equally fundamental. Its long and thin combustion chamber does not burn as ideally as the cylinder of a piston engine. The apex seal must seal a moving chamber while sweeping through housing regions with non-uniform thermal maps. The literature on apex seals identifies gas leakage, wear, vibration, and possible seal lift-off as central problems in rotary engines [6, 7, 8]. Compared with a piston engine, the Wankel engine faces a more difficult sealing problem because its seals do not operate in a simple cylindrical geometry, but along a continuously varying housing trajectory.

The advantage of the conventional piston engine is not merely its historical efficiency, but the predictability of the ring-cylinder system. In a piston engine, ring tension, gas pressure behind the ring, oil film, clearance, and thermal expansion can be calculated within a stable cylindrical path. Modern piston engines can therefore reach high thermal efficiency; Toyota, for example, states that its Dynamic Force Engine achieves 40% thermal efficiency for the conventional petrol variant and 41% for the hybrid variant [4]. The main problem for a new rotary architecture is therefore not simply to increase the number of chambers, but to make the seal and thermal environment sufficiently predictable, in a manner analogous to the piston system.

The *Hexa-Wankel* is proposed as a hypothesis addressing this problem. Its core is not a naive "six-sided Wankel", but a six-apex rotary architecture that uses two phased combustion pulses to stabilise the distribution of heat and pressure. A single fuel dose is divided into two pulses, so the target is not additional energy, but a cleaner conversion of the same chemical energy in terms of torque angle, peak pressure, thermal gradient, and seal load.

2 Design Definition and Hypothesis Statement

2.1 Working definition

In this paper, the term *Hexa-Wankel* denotes the following conceptual design:

1. the rotor has six apexes and six convex sides;
2. the kinematic baseline is Wankel-like: a six-apex rotor moves inside a five-lobe housing obtained from the envelope of apex trajectories;
3. the term "hexa" refers to the number of rotor apexes/chambers, not to the number of housing lobes;
4. two combustion zones are placed at distinct housing-coordinate positions and operate in a phased sequence;
5. the total fuel per cycle is not doubled, but divided into two pulses:

$$Q_{tot} = Q_1 + Q_2, \qquad Q_1 = Q_2 = \frac{1}{2} Q_{tot}. \tag{1}$$

Under this definition, the *Hexa-Wankel* creates no additional energy. The claim is that the same chemical energy may be converted with lower peak stress, lower thermal variance, and lower leakage.

2.2 Sequential-cycle interpretation

The intuitive design interpretation can be stated more simply. A conventional triangular Wankel may be understood, at a schematic level, as a repeating three-stage rotary process:

$$\text{intake} \rightarrow \text{compression/ignition/expansion} \rightarrow \text{exhaust}. \tag{2}$$

The *Hexa-Wankel* hypothesis proposes that a single six-apex curved rotor can carry two such Wankel-like sequences in one integrated rotary architecture:

$$(1, 2, 3) + (4, 5, 6), \tag{3}$$

where

$$\begin{aligned} 1 &= \text{fuel intake}, \quad 2 = \text{compression–ignition–expansion}, \quad 3 = \text{exhaust}, \\ 4 &= \text{fuel intake}, \quad 5 = \text{compression–ignition–expansion}, \quad 6 = \text{exhaust}. \end{aligned} \tag{4}$$

This statement should not be read as two complete triangular Wankel engines mechanically joined together. It is a functional analogy: one six-apex rotor in one five-lobe working track carries two sequential three-stage working patterns. In housing coordinates these are assigned to two combustion regions, denoted Z_R and Z_L, with two fuel inlets, two ignition points, and two exhaust outlets. The design burden is then precise: processes 2 and 5 must occur during positive-expansion intervals of their respective chamber-volume curves.

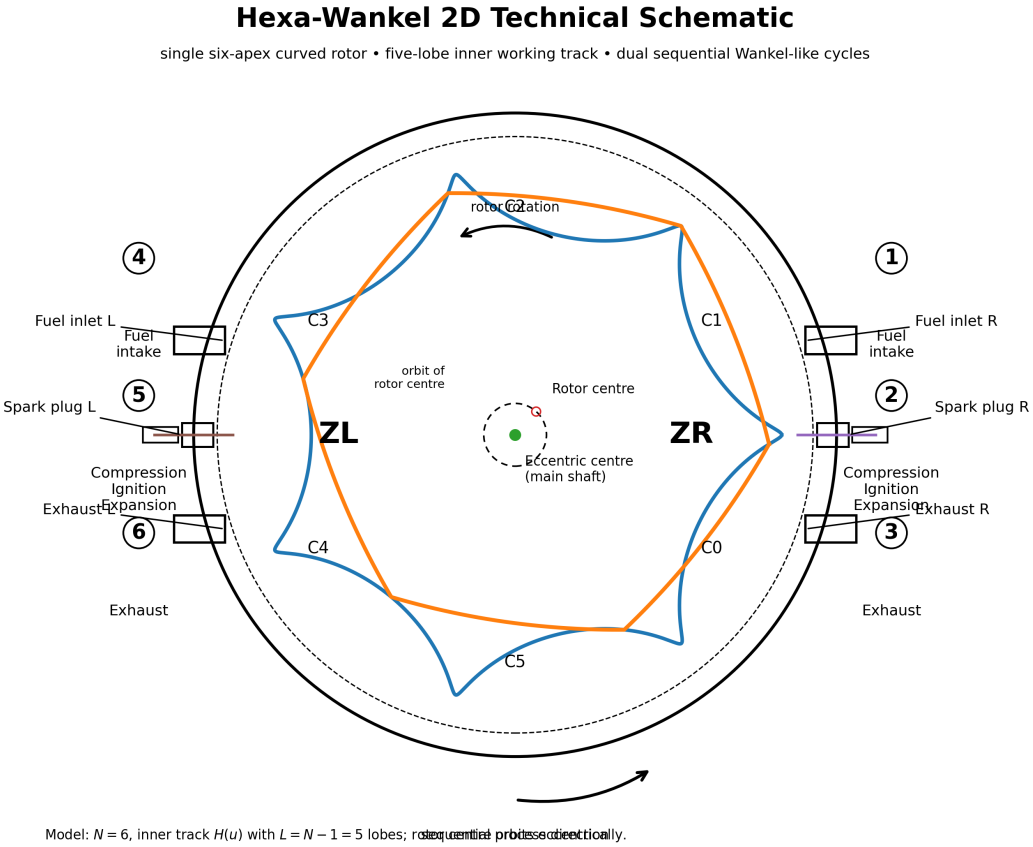

Figure 1: Two-dimensional technical schematic of the proposed *Hexa-Wankel* layout. The figure is a conceptual kinematic layout: a single six-apex curved rotor operates inside a five-lobe inner working track, while two opposed regions Z_R and Z_L carry the sequential process logic $1 \to 2 \to 3$ and $4 \to 5 \to 6$. It is not a production port design.

2.3 Main hypothesis

> If a six-apex rotor in a five-lobe housing can produce sealed chambers with a competitive compression ratio, two positive expansion windows, sufficient gas exchange, and a more stable thermal map, then two combustion pulses $Q/2 + Q/2$ may allow a rotary engine to approach piston-like seal predictability while retaining Wankel-like power density.

The operative word is "if". This paper does not assert that the *Hexa-Wankel* is necessarily more efficient. It derives the threshold conditions under which the claim is not physically empty.

3 Kinematic Closure: Six-Apex Rotor in a Five-Lobe Housing

3.1 Reference case: the conventional Wankel

In the conventional Wankel engine, a three-apex rotor moves inside a two-lobe housing. The internal gearing constrains the eccentric shaft to rotate three times for one material revolution of the rotor [5, 1]. In other words, the rotor apex count $N = 3$ is associated with a two-lobe housing and a shaft-to-rotor speed ratio of $3 : 1$.

To remove geometric ambiguity, this paper adopts the following Wankel-like generalisation as its baseline:

$$N = 6, \qquad L = N - 1 = 5, \tag{5}$$

where N is the number of rotor apexes and L is the number of housing lobes. The baseline *Hexa-Wankel* is therefore:

$$\boxed{\text{six-apex rotor in a five-lobe Wankel-like housing.}} \tag{6}$$

This choice is essential. Without kinematic closure, chamber volume, phase angle, port timing, and thermal balancing would not refer to the same mechanical object.

3.2 Baseline motion law

Let θ_s be the eccentric-shaft angle relative to the housing. The rotor centre travels around a circle of eccentricity e:

$$\boldsymbol{C}(\theta_s) = e \begin{pmatrix} \cos\theta_s \\ \sin\theta_s \end{pmatrix}. \tag{7}$$

For a Wankel-like N-apex baseline, the material orientation of the rotor relative to the housing is written as:

$$\psi(\theta_s) = -\frac{\theta_s}{N} + \psi_0. \tag{8}$$

For the *Hexa-Wankel*, $N = 6$, hence:

$$\psi(\theta_s) = -\frac{\theta_s}{6} + \psi_0. \tag{9}$$

The shaft therefore performs six revolutions for one material revolution of the rotor. This is the baseline kinematic assumption. Mechanically, the law may be represented by a fixed gear and an internal rotor gear with a $5:6$ tooth ratio in the Wankel-like sense: the fixed sun gear has $5q$ teeth and the internal rotor gear has $6q$ teeth for some manufacturing-suitable integer q. This ratio is not a detailed tooth-profile specification, but the minimal kinematic closure required for a six-apex rotor to operate against a five-lobe housing. Other conjugate-pair designs may employ different motion laws, but they are not treated as the main design in this paper.

The six local rotor apexes are defined as:

$$\boldsymbol{a}_k = \rho_k \begin{pmatrix} \cos\alpha_k \\ \sin\alpha_k \end{pmatrix}, \qquad \alpha_k = \frac{2\pi k}{6}, \quad k = 0, \ldots, 5. \tag{10}$$

For a first-order symmetric rotor, $\rho_k = \rho$. The global position of apex k is:

$$\boldsymbol{A}_k(\theta_s) = \boldsymbol{C}(\theta_s) + \boldsymbol{R}(\psi(\theta_s))\boldsymbol{a}_k, \tag{11}$$

where $\boldsymbol{R}$ is the two-dimensional rotation matrix. The first contact-envelope locus generated by the six apex trajectories is:

$$\mathcal{L}_A = \overline{\{\boldsymbol{A}_k(\theta_s) : k = 0, \ldots, 5,\ \theta_s \in [0, 2\pi N)\}}. \tag{12}$$

The manufacturable housing profile $\mathcal{H}$ is not defined merely as the boundary of a set of plotted points. It is the regular closed curve selected from this apex locus under continuous-contact and no-interference constraints. If $\Omega_R(\theta_s)$ denotes the instantaneous rotor domain and Ω_H denotes the housing domain, the required geometric conditions are:

$$\Omega_R(\theta_s) \subseteq \Omega_H, \qquad \boldsymbol{A}_k(\theta_s) \in \mathcal{H} \text{ at intended apex contacts}, \qquad \Omega_R(\theta_s) \cap \Omega_H^c = \varnothing, \tag{13}$$

for all relevant shaft angles. Equations (12) and (13) give a stricter design target than the conceptual drawing. The present paper does not claim that the first-order curve is already a final manufacturing profile; it specifies the envelope and non-interference conditions that a final CAD model must satisfy.

3.3 Consistency between housing and rotor coordinates

Two different coordinates must be separated:

1. housing coordinates, where ports and combustion zones are fixed;
2. rotor/shaft coordinates, where the chamber work phase angle is calculated.

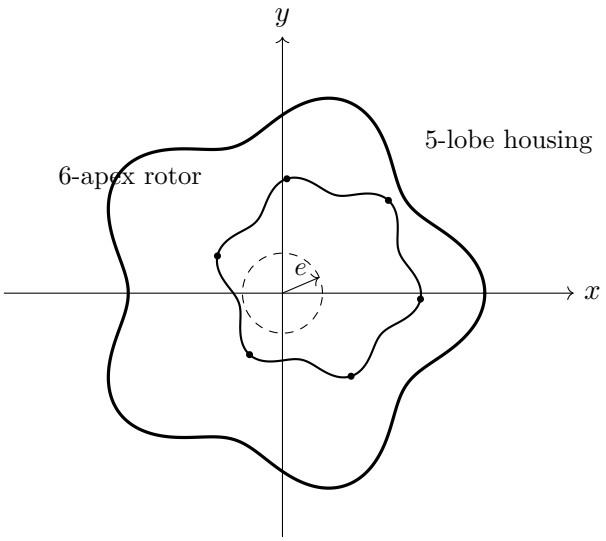

Figure 2: Initial *Hexa-Wankel* schematic as a kinematic baseline: six rotor apexes/chambers inside a five-lobe Wankel-like housing.

Because $\psi(\theta_s) = -\theta_s/N$, the optimum phase angle for mechanical work is not automatically the same as a 180° separation in the housing. The two opposed combustion zones in housing coordinates should therefore be read as a thermal-balancing target, whereas their compatibility with $\Delta\phi^*$ must be calculated from $V_i(\theta_s)$ and $K_i(\theta_s)$.

3.4 Baseline firing sequence

To remove operational ambiguity, this paper uses the following baseline firing sequence. The labels $1, \ldots, 6$ used in the sequential-cycle diagram denote process stages, not fixed chamber identities. By contrast, $C_0, \ldots, C_5$ or $i = 0, \ldots, 5$ denote moving geometric chambers associated with the six-apex rotor. Thus the process logic $1 \to 2 \to 3 + 4 \to 5 \to 6$ is a staged thermodynamic sequence, while the chamber indices identify the geometric chambers that successively pass through the fixed housing zones.

The six chambers are indexed $i = 0, \ldots, 5$ following the rotor-apex order. The right combustion zone Z_R serves the even-indexed chambers $(0, 2, 4)$, whereas the left combustion zone Z_L serves the odd-indexed chambers $(1, 3, 5)$. Consequently, the $Q/2 + Q/2$ fuel split is not defined for a single chamber, but for an equivalent event pair, for example one even event at Z_R and the following odd event at Z_L.

$$Q_{\text{pair}} = Q_R + Q_L, \qquad Q_R \simeq Q_L \simeq \frac{1}{2} Q_{\text{pair}}, \tag{14}$$

with a candidate mechanical offset $\Delta\phi$ to be selected so that both pulses fall within the positive part of the torque kernel. At the chamber-individual level, even chambers receive their pulse from Z_R and odd chambers receive their pulse from Z_L; what is compared with one triangular Wankel pulse is the effective event pair Q_{pair}, not twice the fuel. This scheme is not intended to be the only possible firing order, but an analytical baseline: even and odd chambers are separated so that the two housing zones can provide thermal balancing, while mechanical optimisation remains determined by $K_i(\theta_s) = \mathrm{d}V_i/\,\mathrm{d}\theta_s$.

4 Envelope Geometry and Regularity

4.1 Initial curve family

For first-order analysis, the following trochoidal/peritrochoidal curve family is used:

$$\boldsymbol{H}_n(\theta) = R\begin{pmatrix}\cos\theta\\ \sin\theta\end{pmatrix} + e\begin{pmatrix}\cos n\theta\\ \sin n\theta\end{pmatrix}, \qquad 0 \le \theta < 2\pi. \tag{15}$$

Drogosz emphasises that Wankel geometry must be formalised mathematically because the housing curve, rotor, and eccentricity parameters determine the chamber geometry [1]. Equation (15) is not the final profile, but a scaling law for regularity and initial displacement. The final housing profile must still be calculated from the contact-envelope and no-interference constraints in Equations (12)–(13); in other words, $\boldsymbol{H}_n(\theta)$ is a first-order approximation for studying regularity limits and displacement scale, not a substitute for the actual chamber boundary. Since the baseline *Hexa-Wankel* uses a six-apex rotor in a five-lobe housing, every final volume figure must be derived from the rotor-housing pair in Equations (11)–(13), not from $\boldsymbol{H}_n$ alone.

The derivative is:

$$\boldsymbol{H}_n'(\theta) = R\begin{pmatrix}-\sin\theta\\ \cos\theta\end{pmatrix} + ne\begin{pmatrix}-\sin n\theta\\ \cos n\theta\end{pmatrix}. \tag{16}$$

Its norm is:

$$\left\|\boldsymbol{H}_n'(\theta)\right\|^2 = R^2 + n^2e^2 + 2nRe\cos((n-1)\theta). \tag{17}$$

The minimum occurs when $\cos((n-1)\theta) = -1$, hence:

$$\min_\theta \left\|\boldsymbol{H}_n'(\theta)\right\| = |R - ne|. \tag{18}$$

The no-cusp condition is therefore:

$$\boxed{R > ne.} \tag{19}$$

For the six-apex candidate:

$$R > 6e. \tag{20}$$

If $R = 105\,\text{mm}$, then:

$$e < 17.5\,\text{mm}. \tag{21}$$

With a conservative eccentricity $e_H = 7.5$–$10\,\text{mm}$, the regularity margin is greater than with $e = 15\,\text{mm}$.

4.2 Status of the displacement formula

The first-order swept-volume formula used here is:

$$V_{d,n} \simeq 2nbRe \sin\left(\frac{2\pi}{n}\right), \tag{22}$$

where b is the rotor width/depth. This formula must be read as a *scaling law*, not as a substitute for chamber-volume computation. The final displacement must be calculated from the actual chamber area:

$$V_i(\theta_s) = bA_i(\theta_s). \tag{23}$$

For $n = 3$:

$$V_{d,3} = 6bRe \sin\left(\frac{2\pi}{3}\right) = 3\sqrt{3}bRe, \tag{24}$$

which is consistent with the usual form of the Wankel displacement formula. For $n = 6$:

$$V_{d,6} = 12bRe \sin\left(\frac{2\pi}{6}\right) = 6\sqrt{3}bRe. \tag{25}$$

Thus, at the same R, e, and b:

$$\frac{V_{d,6}}{V_{d,3}} = 2. \tag{26}$$

This result must not be read as proof of doubled efficiency. It means only that, for the same effective displacement, the six-apex candidate may reduce either e or b.

4.3 Scaling for equal effective displacement

To give the six-apex candidate an effective displacement equivalent to the three-apex reference, three scaling strategies are available:

Strategy	First-order condition	Design consequence
width reduction	$b_H = \frac{1}{2}b_W$	axially shorter engine
eccentricity reduction	$e_H = \frac{1}{2}e_W$	improved orbit, sliding severity, and regularity margin
hybrid scaling	$b_H e_H = \frac{1}{2}b_W e_W$	compromise between packaging and tribology

Table 1: Scaling strategies for equalising the effective displacement of the six-apex candidate and the three-apex reference.

Take, for example:

$$R = 105\,\text{mm}, \quad e_W = 15\,\text{mm}, \quad b = 80\,\text{mm}. \tag{27}$$

Then:

$$V_{d,3} = 3\sqrt{3}(0.080)(0.105)(0.015) \tag{28}$$
$$\approx 6.55 \times 10^{-4}\,\mathrm{m}^3 \tag{29}$$
$$\approx 655\,\mathrm{cc}. \tag{30}$$

For $n = 6$ with $e_H = 7.5\,\mathrm{mm}$:

$$V_{d,6} = 6\sqrt{3}(0.080)(0.105)(0.0075) \tag{31}$$
$$\approx 655\,\mathrm{cc}. \tag{32}$$

At equal effective displacement, the six-apex candidate can therefore use half the eccentricity of the three-apex reference. This provides a physical basis for the hypothesis of reduced sliding severity, but it does not yet prove leakage reduction or efficiency improvement.

5 Compression Ratio from Chamber Volume

Compression ratio must not be assumed from a target value. It must be calculated from the actual chamber volume:

$$r_i = \frac{V_{i,\max}}{V_{i,\min}} = \frac{V_{c,i} + V_{d,i}}{V_{c,i}}. \tag{33}$$

With $V_d = 655\,\mathrm{cc}$, a target $r = 10.5$ requires:

$$V_c = \frac{V_d}{r-1} = \frac{655}{9.5} = 68.9\,\mathrm{cc}. \tag{34}$$

This clearance corresponds to:

$$\frac{V_c}{V_d} = 0.105. \tag{35}$$

A target $r = 10.5$ therefore means that the minimum volume must be approximately 10.5% of the swept volume. This is plausible as an order-of-magnitude target, but it does not prove that the six-apex/five-lobe housing can achieve it. The geometric criterion to be satisfied is:

$$r_{H,i} = \frac{\max_{\theta_s} A_i(\theta_s)}{\min_{\theta_s} A_i(\theta_s)} \geq 10. \tag{36}$$

If CAD gives $r_{H,i} < 9$, then the high-efficiency claim fails or requires modification through a rotor pocket, flank curvature, or variable-compression geometry.

6 Initial Kinematic CAD Validation and Actual Chamber Volume

To test whether the kinematic definition in Section 3 can generate actual computable chambers, a first-order two-dimensional kinematic CAD model was produced. This model is not a final manufacturing CAD, but an initial geometric validation of two features: the housing-rotor form and the chamber-volume curves $V_i(\theta)$.

The model parameters are:

$$N = 6, \qquad L = 5, \qquad R = 60\,\text{mm}, \qquad e = 8\,\text{mm}, \qquad b = 80\,\text{mm}. \tag{37}$$

The regularity condition is satisfied because:

$$R > Ne, \qquad 60 > 48. \tag{38}$$

The housing is calculated from the five-lobe envelope trajectory, whereas the rotor is represented as six convex flanks with six apex contact points. Chamber area i is calculated from the closed polygon between the corresponding housing segment and rotor flank. The volume is obtained as:

$$V_i(\theta) = bA_i(\theta), \tag{39}$$

where $A_i(\theta)$ is the numerical chamber area in mm^2 and b is the rotor width in mm. Conversion to cc uses:

$$V_{i,cc}(\theta) = \frac{bA_i(\theta)}{1000}. \tag{40}$$

The raw numerical result indicates that all chambers are symmetric, with the following values:

Model	V_{min}	V_{max}	V_d	r_{raw}
Raw geometric chamber	0.053 cc	35.839 cc	35.786 cc	672.1
Clearance-corrected $r = 10.5$	3.767 cc	39.552 cc	35.786 cc	10.5

Table 2: Actual chamber-volume validation for the baseline $R = 60\,\text{mm}$, $e = 8\,\text{mm}$, and $b = 80\,\text{mm}$. The raw value must not be read as a real engine compression ratio because it does not include a combustion pocket or clearance volume.

The important finding is that the ideal geometry without a pocket gives a near-zero V_{min}. Hence the raw compression ratio $r_{raw} \approx 672$ is unrealistic and must not be used as a performance claim. The design-relevant result is the required additional clearance:

$$V_{c,add} = \frac{V_d}{r_t - 1} - V_{min,raw}, \tag{41}$$

where $r_t = 10.5$. With $V_d = 35.786\,\text{cc}$ and $V_{min,raw} = 0.053\,\text{cc}$, one obtains:

$$V_{c,add} = 3.714\,\text{cc}. \tag{42}$$

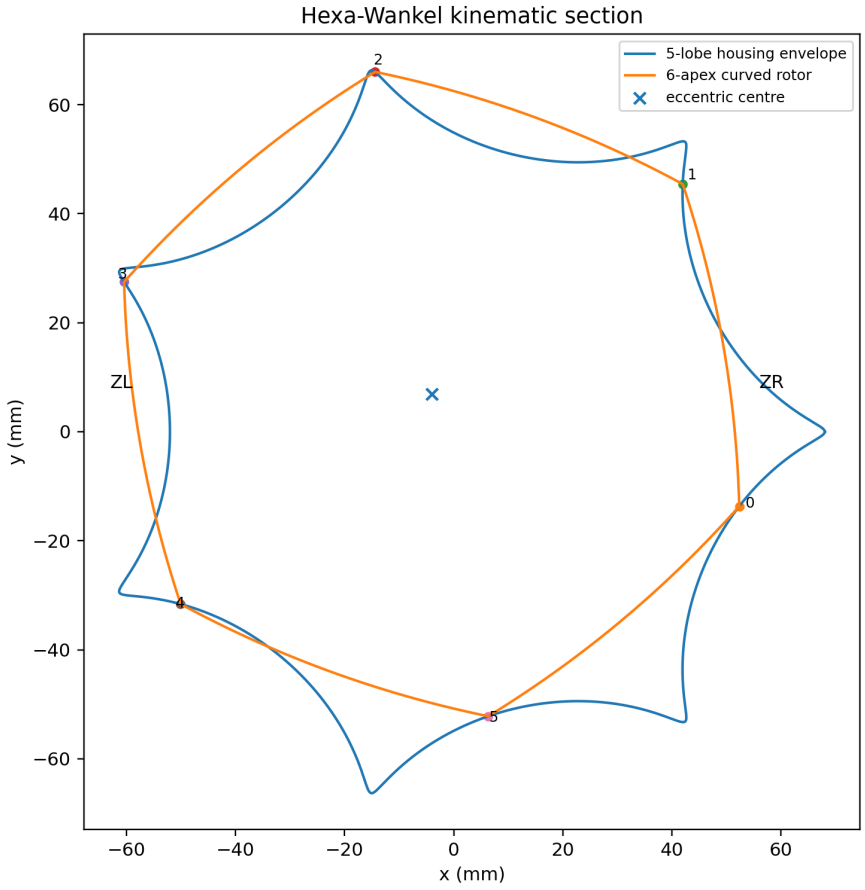

Figure 3: Two-dimensional kinematic CAD validation: a six-apex rotor within the baseline five-lobe housing. ZR and ZL denote two fixed combustion zones in housing coordinates.

The corrected minimum volume becomes:

$$V_{min,corr} = 3.767\,\text{cc}, \tag{43}$$

and the corrected maximum volume becomes:

$$V_{max,corr} = 39.552\,\text{cc}. \tag{44}$$

The initial kinematic CAD model therefore supports two limited conclusions. First, actual chambers can be defined and numerically calculated in the six-apex/five-lobe baseline. Second, the target $r = 10.5$ does not arise automatically from the ideal envelope, but requires an explicit combustion-pocket or clearance-volume design. This strengthens the paper's position: compression ratio is a geometric requirement to be designed, not a performance assumption.

A combustion pocket is not merely a mathematical volume addition. In a real engine, the pocket must be located and shaped so that it does not create a large dead volume, excessive flame travel, strong near-wall quenching, or increased hydrocarbon loss. The clearance-corrected result in Table 2 must therefore be read as a combustion-chamber geometry target, not as proof that combustion is already efficient. Pocket design is one of the decisive issues for the *Hexa-Wankel* before CFD analysis can be undertaken.

6.1 Limits of interpretation of the 2D model

The results in Section 6 must be read strictly as two-dimensional geometric validation, not as engine-performance validation. The model shows that chambers can be formed and actual volume $V_i(\theta)$ can be computed, but it does not show that dual-zone sequential combustion, three-dimensional sealing, gas exchange, or thermal deformation will work better than in a Wankel or piston engine.

There are five main limits. First, the model remains two-dimensional: it does not include side-housing thickness, corner seals, side seals, oil film, axial thermal expansion, or housing deformation. Second, the additional clearance of 3.714 cc per chamber, approximately 10.4% of V_d, is not a defect in itself, but it is a combustion-pocket design burden. The pocket shape must preserve compression ratio without excessive surface-to-volume ratio, quenching, or hydrocarbon loss. Third, phased combustion has not yet been verified against the actual torque kernel. A 180° separation in housing coordinates provides only a thermal-balancing target; it must be tested against $K_i(\theta) = \mathrm{d}V_i/\,\mathrm{d}\theta$ so that both pulses occur during positive expansion windows. Fourth, port timing is still represented by a worst-case estimate; with six chambers, intake and exhaust duration per chamber may become shorter and may reduce volumetric efficiency. Fifth, the model scale remains small, with $V_d \approx 35.8\,\text{cc}$ per chamber. Scaling up to a total engine of 650–1300 cc must be recalculated because surface-to-volume ratio, seal force, sliding velocity, thermal distortion, and cooling requirements do not scale linearly.

The present validation status is therefore: basic 2D geometry passes, chamber-volume computability passes, preliminary torque-kernel phase placement passes, and an idealised zero-dimensional indicated-work test gives positive indicated work. Final engine final performance does not yet pass, because brake power, BSFC, BTE, production sealing, real port gas exchange, CFD combustion, FEA thermal distortion, and dynamometer results have not been established.

Validated at this stage	**Not yet validated / next stage**
Six-apex/five-lobe kinematic closure and baseline gear law	Torque, power, BSFC, or BTE advantage over Wankel/piston engines
Periodic chamber formation in the 2D model	Final conjugate flank optimisation and production sealing geometry
Actual chamber-volume computation $V_i(\theta)$	Actual port timing, scavenging, and volumetric efficiency
Required clearance volume for target $r \approx 10.5$	Combustion-pocket design, flame travel, quenching, and HC loss
Preliminary torque-kernel extraction $K_i = \mathrm{d}V_i/\mathrm{d}\theta_s$	CFD combustion and wall heat-transfer validation
Positive-K_i candidate windows in Z_R and Z_L	FEA thermal distortion and full apex-corner-side seal dynamics
Idealised 0-D indicated-work model with $W = \int p\,\mathrm{d}V > 0$	Brake work, friction mean effective pressure, BSFC, BTE, and dynamometer testing

Table 3: Validation status of the present paper. The table separates results shown by the 2D kinematic, torque-kernel, and idealised indicated-work models from final performance claims that still require testing.

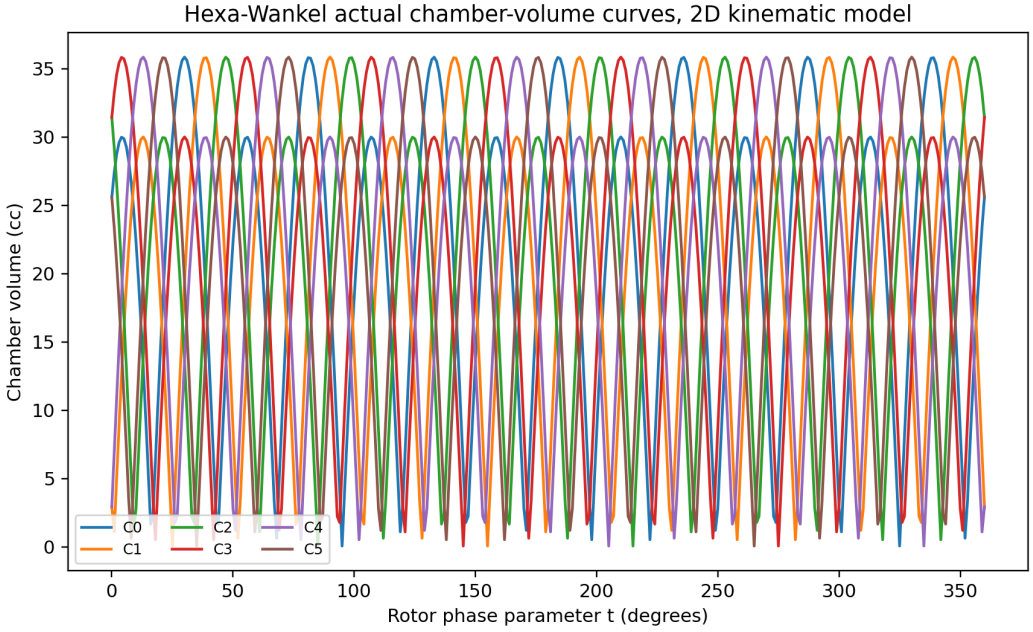

Figure 4: Raw chamber-volume curves from the 2D kinematic model. The near-zero minimum volume shows why a real design must include a combustion pocket or clearance volume.

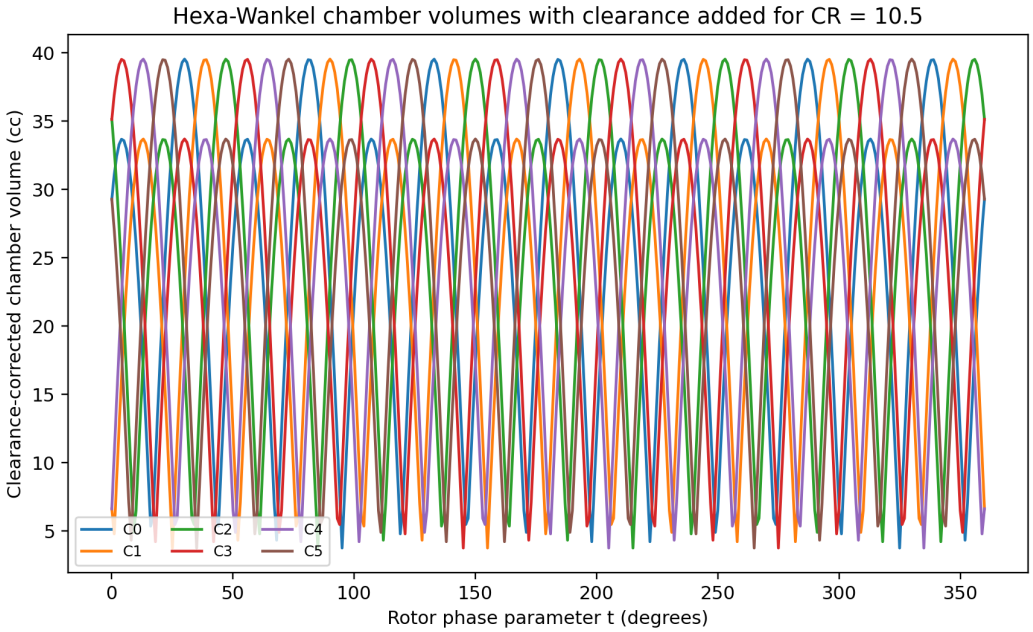

Figure 5: Clearance-corrected chamber-volume curves for the target compression ratio $r = 10.5$. These curves are suitable for torque-kernel extraction, but not by themselves for performance prediction.

7 Preliminary Torque-Kernel Validation of the Sequential-Cycle Hypothesis

The preceding volume model proves only that the six chambers can be represented and that their volumes vary periodically. The next question is stricter: whether the proposed process sequence $1 \to 2 \to 3 + 4 \to 5 \to 6$ can place its two combustion/expansion events inside mechanically favourable parts of the volume curve.

For this purpose, the clearance-corrected chamber-volume functions were numerically differentiated with respect to shaft angle:

$$K_i(\theta_s) = \frac{\mathrm{d}V_i}{\mathrm{d}\theta_s}. \tag{45}$$

Since positive indicated work requires $\mathrm{d}W = p\,\mathrm{d}V > 0$, a candidate combustion event is kinematically plausible only where

$$K_i(\theta_s) > 0. \tag{46}$$

The numerical validation therefore used three quantities: the chamber volume $V_i(\theta_s)$, the chamber centroid angle in housing coordinates, and the torque kernel $K_i(\theta_s)$. Candidate right-zone and left-zone events were accepted only when the chamber centroid lay within the corresponding housing-coordinate zone and the torque kernel was positive. This does not assume a pressure trace; it tests the necessary geometric condition that pressure rise must coincide with expansion rather than compression.

This result changes the status of the hypothesis. The paper no longer relies only on visual geometry or symbolic volume scaling; it now includes a first numerical test of whether the proposed two sequential Wankel-like cycles can be synchronised with expansion-positive

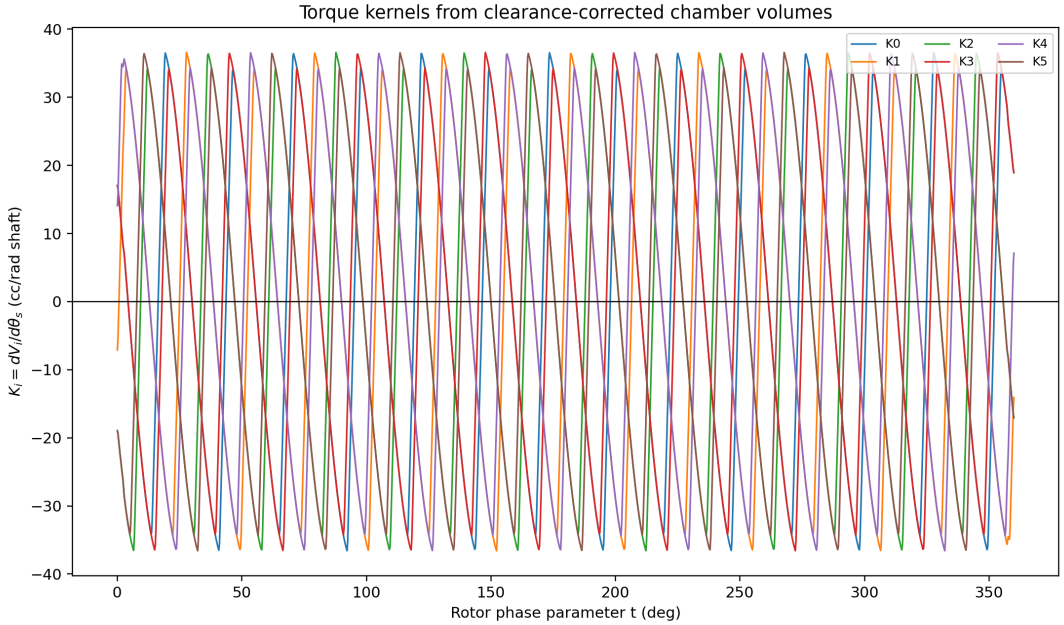

Figure 6: Preliminary torque kernels $K_i = \mathrm{d}V_i/\,\mathrm{d}\theta_s$ obtained by differentiating the clearance-corrected chamber-volume curves. Positive portions of these curves are the only intervals capable of converting combustion pressure into positive indicated work.

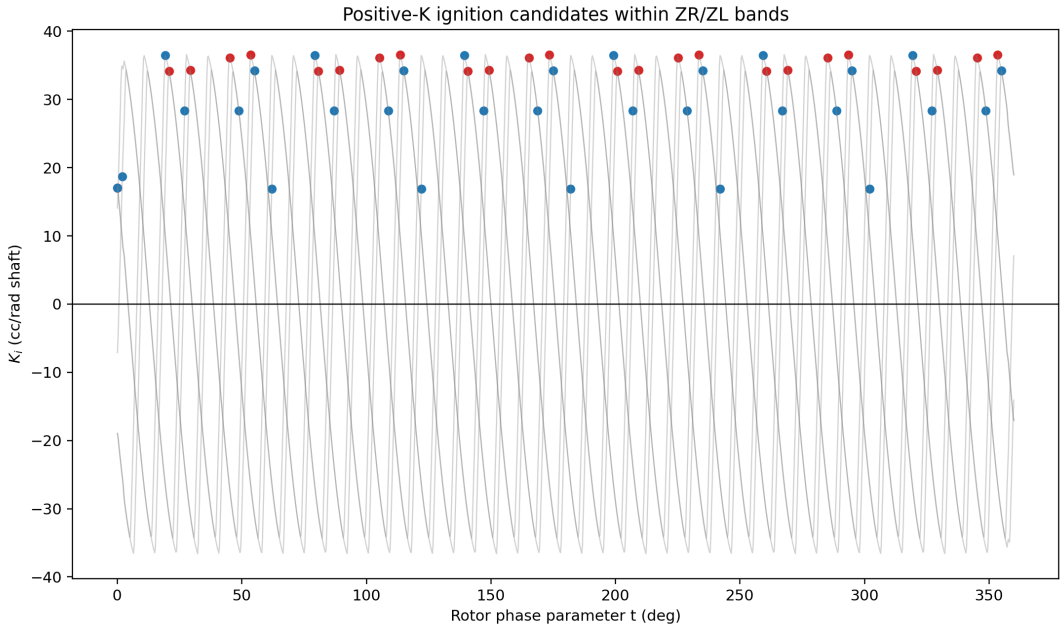

Figure 7: Candidate ignition/expansion placements in the right and left combustion-zone bands, overlaid on the torque-kernel field. The result supports the limited claim that the sequential-cycle logic is not geometrically self-defeating: processes 2 and 5 can, in principle, be placed within positive-K_i windows.

windows. The result is positive at the kinematic level: the six chambers possess positive-K_i intervals, and right/left combustion candidates can be assigned to such intervals.

The claim remains deliberately narrow. The torque-kernel test does not prove brake power, brake specific fuel consumption, brake thermal efficiency, or superiority over a triangular Wankel. It establishes only that the $1 \to 2 \to 3+4 \to 5 \to 6$ sequence is not ruled out by the chamber-volume derivative. The following section therefore adds the next theoretical layer: a zero-dimensional pressure model $p_i(\theta)$ and an indicated-work calculation.

8 Indicated Work and Phase Angle

Throughout this section, θ denotes shaft angle, i.e. $\theta = \theta_s$, unless explicitly stated otherwise.

For any rotary chamber, the indicated work is:

$$W_i = \oint p_i(\theta)\,\mathrm{d}V_i(\theta). \tag{47}$$

The torque contribution can be written as:

$$\tau_i(\theta) = p_i(\theta)\frac{\mathrm{d}V_i}{\mathrm{d}\theta}. \tag{48}$$

Define the chamber torque kernel:

$$K_i(\theta) = \frac{\mathrm{d}V_i}{\mathrm{d}\theta}. \tag{49}$$

Only intervals for which $K_i(\theta) > 0$ can produce positive expansion work. A dual-pulse combustion strategy is therefore mechanically meaningful only if both pulses are placed on positive and sufficiently large sections of K_i.

For the triangular *Wankel* reference, a simplified single-pulse work model is:

$$W_W \approx \int_{\theta_a}^{\theta_b} p_W(\theta) K_W(\theta)\,\mathrm{d}\theta. \tag{50}$$

For the *Hexa-Wankel* two-pulse candidate, the fuel split is placed in the pressure trace itself rather than added as an external factor. Thus, if $Q_R = Q_L = Q_{pair}/2$, the mechanically relevant work model is:

$$\begin{aligned} W_H(\Delta\phi) = &\int_{\theta_a}^{\theta_b} p_R^{(Q_R)}(\theta) K_R(\theta)\,\mathrm{d}\theta \\ &+ \int_{\theta_a}^{\theta_b} p_L^{(Q_L)}(\theta+\Delta\phi) K_L(\theta+\Delta\phi)\,\mathrm{d}\theta, \end{aligned} \tag{51}$$

where the superscript indicates the fuel energy used to generate the pressure trace. No additional factor of 1/2 appears in Equation (51), because each pressure trace already corresponds to its half-fuel event.

The optimum mechanical phase angle is therefore:

$$\Delta\phi^* = \arg\max_{\Delta\phi} W_H(\Delta\phi). \tag{52}$$

This is not merely the statement that the best phase is the best phase, because $K_i(\theta)$ must be obtained from the actual chamber geometry. Once $V_i(\theta)$ is computed by CAD, Equation (52) becomes a numerical test. If the optimum $\Delta\phi^*$ conflicts with the 180° thermal-balancing separation in housing coordinates, the design must be revised.

8.1 Preliminary zero-dimensional indicated-work model

The torque-kernel validation supplies a necessary kinematic condition, but not a pressure trace. The next test is therefore to couple the computed clearance-corrected chamber volume to a minimal zero-dimensional thermodynamic model. For this step the unsmoothed clearance-corrected volume curve is used; smoothing is deliberately avoided because it changes V_{min} and therefore alters the effective compression ratio.

The indicated work of chamber i is calculated as

$$W_i = \int_{\theta_a}^{\theta_b} p_i(\theta)\frac{\mathrm{d}V_i}{\mathrm{d}\theta}\,\mathrm{d}\theta = \int_{\theta_a}^{\theta_b} p_i(\theta)K_i(\theta)\,\mathrm{d}\theta. \tag{53}$$

The single-zone ideal-gas model is:

$$p_i(\theta) = \frac{m_i R T_i(\theta)}{V_i(\theta)}, \tag{54}$$

$$\frac{\mathrm{d}T_i}{\mathrm{d}\theta} = \frac{1}{m_i c_v}\left(\frac{\mathrm{d}Q_i}{\mathrm{d}\theta} - p_i(\theta)\frac{\mathrm{d}V_i}{\mathrm{d}\theta}\right). \tag{55}$$

Heat release is represented by a finite-duration Wiebe function. To avoid domain ambiguity before ignition and after the prescribed burn interval, the burned fraction is defined piecewise:

$$x_b(\theta) = \begin{cases} 0, & \theta < \theta_{ign}, \\ 1 - \exp\left[-a\left(\dfrac{\theta - \theta_{ign}}{\Delta\theta_b}\right)^{m_w+1}\right], & \theta_{ign} \le \theta \le \theta_{ign} + \Delta\theta_b, \\ 1 - \exp(-a), & \theta > \theta_{ign} + \Delta\theta_b. \end{cases} \tag{56}$$

The heat-release rate is then

$$\frac{\mathrm{d}Q_i}{\mathrm{d}\theta} = Q_i\frac{\mathrm{d}x_b}{\mathrm{d}\theta}. \tag{57}$$

The numerical example uses $a = 6.908$ and $m_w = 2$. The total fuel energy assigned to one paired event remains fixed:

$$Q_{pair} = Q_R + Q_L, \qquad Q_R \simeq Q_L \simeq \frac{1}{2}Q_{pair}. \tag{58}$$

The selected representative event uses the following clearance-corrected chamber volumes: $V_{start} = 33.729\,\mathrm{cc}$, $V_{min} = 4.053\,\mathrm{cc}$, and $V_{end} = 39.551\,\mathrm{cc}$. The resulting effective compression

ratio from the compression start to minimum volume is 8.322, while the larger endpoint-to-minimum ratio is 9.758. A timing sweep gives the best screened theoretical case at 5° shaft angle before minimum volume, with a 10° shaft-angle burn duration. These values are not presented as an engine calibration, but as the optimum of the stated idealised 0-D test.

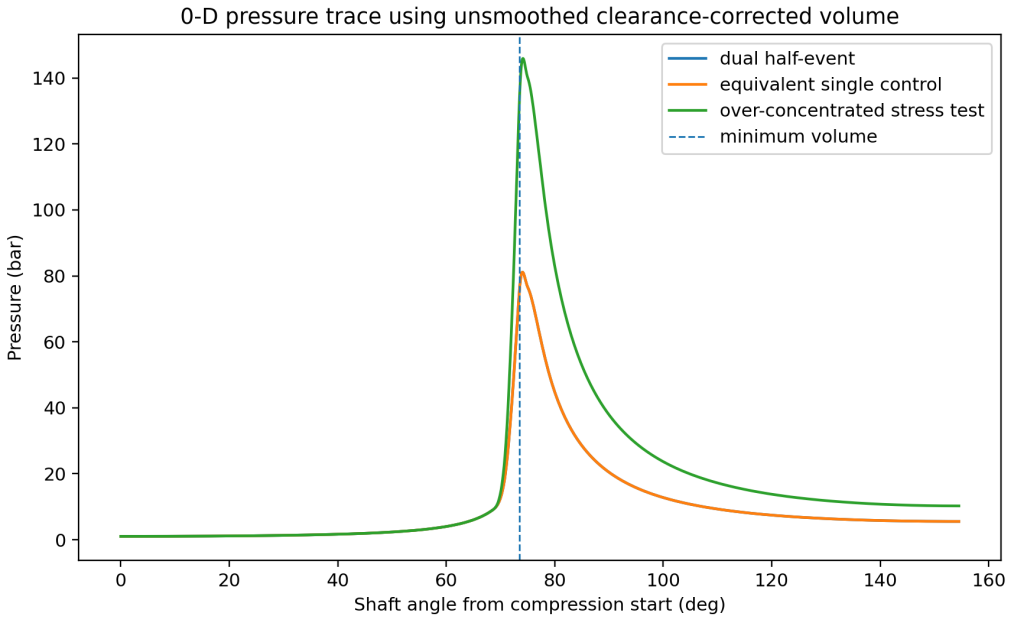

Figure 8: Idealised zero-dimensional pressure trace using the unsmoothed clearance-corrected chamber-volume curve. The fair equivalent-displacement single-pulse control preserves the same fuel-air ratio and compression ratio, and therefore gives essentially the same ideal pressure trace. The over-concentrated single-pulse stress test is not a fair efficiency control; it illustrates the pressure penalty of placing the paired fuel energy into one half-event chamber.

Case	W **(J)**	η_i **(%)**	p_{max} **(bar)**	**IMEP (bar)**	**RI**
Hexa-Wankel dual-pulse pair	120.05	53.18	81.14	20.23	2.74
Equivalent-displacement single-pulse control	120.05	53.18	81.14	20.23	4.02
Over-concentrated single-pulse stress test	119.51	52.94	145.95	40.27	–

Table 4: Preliminary 0-D indicated-work results. The indicated efficiency is an ideal no-wall-loss value, not brake thermal efficiency. The fair equivalent-displacement control has the same ideal work because it preserves compression ratio and fuel-air ratio. The main supported advantage of the dual-pulse case is lower theoretical torque concentration, not a guaranteed increase in ideal efficiency.

The model therefore supports a narrower but important claim:

$$W_H = 120.05\,\mathrm{J} > 0, \tag{59}$$

so the *Hexa-Wankel* is not defeated by the pressure-volume relation in this idealised closed-cycle calculation. At the same time, the fair equivalent-displacement single-pulse control gives essentially identical ideal indicated work and peak pressure. Therefore the present calculation does not support an automatic efficiency advantage. It supports positive indicated work and work redistribution.

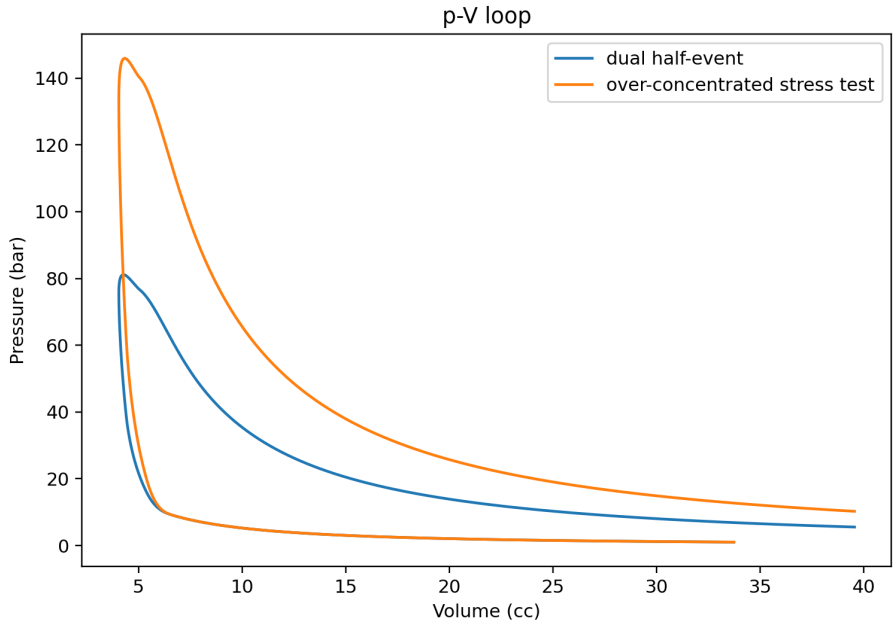

Figure 9: Idealised p-V loop for the dual half-event and the over-concentrated single-pulse stress test. The loop demonstrates positive indicated work, but it is a no-wall-loss 0-D result rather than brake work.

The phase-smoothing calculation compares a concentrated single event with two separated half-events. The theoretical torque-ripple index is

$$RI = \frac{\sigma_\tau}{\bar{\tau}}, \tag{60}$$

and the best phase-screened result gives

$$RI_H = 2.74 < RI_S = 4.02. \tag{61}$$

This RI is a waveform-distribution metric. It is not a full torsional-dynamics, bearing-load, or NVH model of the output shaft.

Thus the preliminary indicated-work result is positive but conservative in implication. The *Hexa-Wankel* is not shown to be more efficient than a fair single-pulse control in the ideal 0-D limit. Its strongest supported theoretical advantage is that work can be redistributed into two sequential pulses, reducing torque concentration while keeping the total fuel energy fixed.

8.2 Parametric leakage sensitivity in the pressure model

A first leakage sensitivity calculation was added using a simple orifice approximation,

$$\dot{m}_{leak} = C_d A_{gap} \sqrt{2\rho\Delta p}, \tag{62}$$

where $A_{gap} = bh$ for rotor width b and equivalent gap h. This is not a three-dimensional seal-flow solver; it is a sensitivity test showing how rapidly leakage grows with clearance.

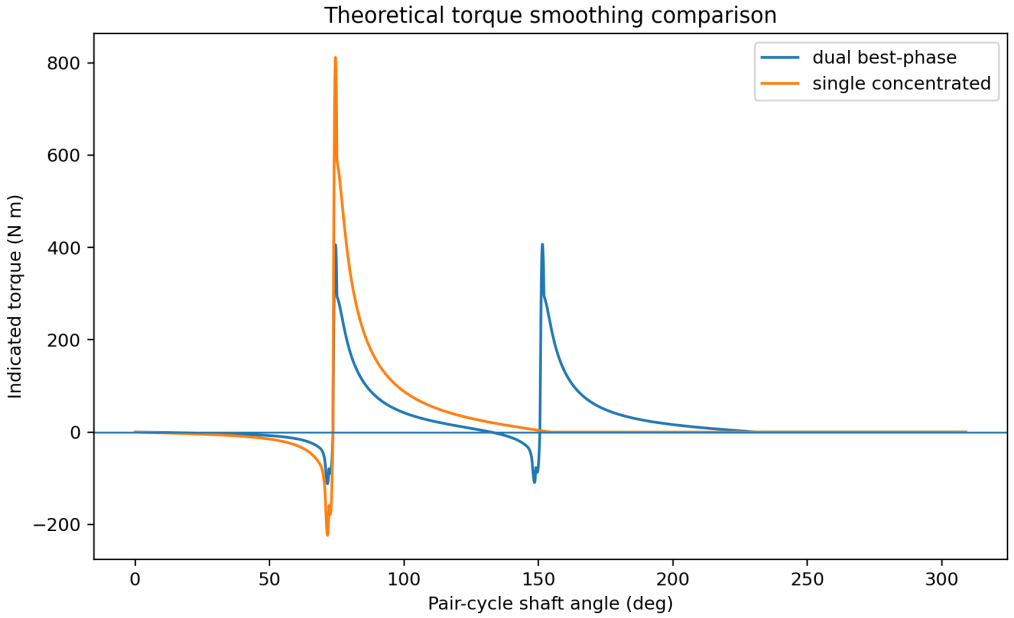

Figure 10: Theoretical torque-smoothing comparison. The dual-pulse case preserves positive indicated work while distributing the torque contribution over two separated events. This is a phase-superposition result, not a full crankshaft torsional model.

Narrow real seal gaps may require laminar thin-gap, Couette-Poiseuille, compressible, or choked-flow treatment depending on pressure ratio, temperature, and gap geometry.

Gap (μm)	A_{gap} **(mm^2)**	**Leaked mass (mg)**	**Leakage (%)**
1	0.08	0.36	0.90
2	0.16	0.71	1.80
5	0.40	1.79	4.50
10	0.80	3.57	9.00
20	1.60	7.14	17.99
40	3.20	14.28	35.98
80	6.40	28.56	71.96

Table 5: Parametric leakage estimate per half-event. The calculation is approximate, but it shows the central engineering condition: the concept remains plausible only if seal clearance is kept small and thermally predictable.

The leakage model strengthens the sealing argument rather than removing it. The *Hexa-Wankel* hypothesis is not that six apexes magically solve leakage. It is that a more periodic and symmetric thermal-pressure map may reduce clearance variability and make seal preload, material, oil film, and cooling design more deterministic. In other words, the sealing problem is not eliminated; it is transformed into a thermal-periodic design problem that can be measured and optimised.

9 Thermal Stabilisation Through Fourier Harmonics

9.1 Not a colder engine

The *Hexa-Wankel* hypothesis is not that the engine is simply colder. A combustion engine must retain sufficient gas temperature during expansion. The relevant target is not lower mean temperature, but lower thermal non-uniformity in the housing:

$$\Delta T_h = \max_{x\in\mathcal{H}} T(x) - \min_{x\in\mathcal{H}} T(x), \tag{63}$$

or, more generally, lower thermal variance:

$$\sigma_T^2 = \frac{1}{|\mathcal{H}|}\int_{\mathcal{H}} (T(x)-\bar{T})^2\,\mathrm{d}x. \tag{64}$$

Let the housing heat-flux distribution from a combustion zone at angular position θ_R be:

$$\dot{q}_R(\theta) = q_0 F(\theta-\theta_R). \tag{65}$$

Expand F as a Fourier series:

$$F(\theta) = \sum_{m=-\infty}^{\infty} F_m e^{im\theta}. \tag{66}$$

If the second combustion zone is placed at:

$$\theta_L = \theta_R + \pi, \tag{67}$$

then the total housing heat flux is:

$$\begin{aligned}
\dot{q}_H(\theta) &= q_0 F(\theta-\theta_R) + q_0 F(\theta-\theta_L) && (68)\\
&= q_0 \sum_m F_m e^{im(\theta-\theta_R)}\left[1+e^{-im\pi}\right] && (69)\\
&= q_0 \sum_m F_m e^{im(\theta-\theta_R)}\left[1+(-1)^m\right]. && (70)
\end{aligned}$$

For odd m:

$$1+(-1)^m = 0. \tag{71}$$

Thus all odd harmonics vanish. The physical interpretation is that two opposed combustion zones can suppress the first-order thermal asymmetry of the housing. This is the strongest mathematical argument for the thermal-stabilisation claim.

This cancellation is exact only under equal-amplitude, identical heat-flux profiles and linear superposition in housing coordinates. In a real engine, conduction delay, coolant geometry, material anisotropy, unequal combustion phasing, and local wall heat transfer can break the ideal cancellation. The Fourier result should therefore be read as a design tendency and a falsifiable thermal-balancing hypothesis, not as a guaranteed thermal outcome.

9.2 Limitation of the Fourier analysis

The cancellation in Equation (70) is a housing-coordinate result. It does not automatically prove mechanical optimality. Mechanical work depends on the rotor/shaft phase angle through $K_i(\theta)$, whereas thermal balancing depends on fixed housing positions. Therefore, the following compatibility condition is necessary:

$$|\Delta\phi^* - \Delta\phi_{thermal}| < \epsilon_\phi, \tag{72}$$

where $\Delta\phi_{thermal}$ is the phase separation implied by the two opposed housing zones after being mapped into the chamber work coordinate. If Equation (72) fails, the thermal and mechanical optima are not aligned.

10 Surface-to-Volume Hazard

Dividing one chamber into two smaller events can reduce peak heat flux, but it can also increase the surface-to-volume ratio. If one chamber of volume V is divided into two geometrically similar chambers of volume $V/2$, then:

$$A_{new} = 2A\left(\frac{1}{2}\right)^{2/3} = 2^{1/3}A \approx 1.26A. \tag{73}$$

This is a 26% increase in total wall area for the same volume. The effect is beneficial only if the reduction in thermal non-uniformity and seal load exceeds the additional wall heat loss. Thus the design condition is:

$$\Delta W_{thermal\ stability} > \Delta Q_{wall\ loss}. \tag{74}$$

This is why the *Hexa-Wankel* must be treated as a threshold theory rather than a claim of automatic efficiency.

11 Seal, Friction, Leakage, and Wear

11.1 Apex-seal force

A first-order apex-seal load model is:

$$F_s = F_{spring} + F_{gas} + F_{inertia}. \tag{75}$$

The contact pressure is:

$$p_c = \frac{F_s}{A_c}. \tag{76}$$

A seal must satisfy two conflicting conditions:

$$F_s > F_{lift-off}, \tag{77}$$

but:

$$F_s \text{ must not be so large that friction and wear dominate.} \tag{78}$$

The *Hexa-Wankel* hypothesis is that a more periodic pressure and thermal map may reduce the required safety margin in F_{spring}.

11.2 Friction threshold

For the triangular Wankel reference, write the total apex friction loss as:

$$P_{f,W} = 3\mu F_W v_W. \tag{79}$$

For the six-apex candidate:

$$P_{f,H} = 6\mu F_H v_H. \tag{80}$$

Define:

$$\lambda_F = \frac{F_H}{F_W}, \qquad \lambda_v = \frac{v_H}{v_W}. \tag{81}$$

For the six-apex candidate not to lose against the triangular Wankel reference in apex friction:

$$P_{f,H} < P_{f,W}. \tag{82}$$

Substitution gives:

$$6\mu F_H v_H < 3\mu F_W v_W, \tag{83}$$

or:

$$\boxed{\lambda_F \lambda_v < 0.5.} \tag{84}$$

This is a severe condition. If $e_H = e_W/2$ reduces sliding severity, a first estimate might suggest a reduced λ_v. However, a value such as $\lambda_v = 0.8$ is a conservative threshold value rather than an optimistic kinematic prediction, because equal output power may require a different shaft speed and dynamic contact condition. If $\lambda_v = 0.8$, then:

$$\lambda_F < 0.625. \tag{85}$$

Therefore the six-apex architecture must reduce effective seal force by more than 37.5% merely to break even in apex-friction loss.

11.3 Leakage threshold and exposure time

For simplified compressible leakage through a small effective gap:

$$\dot{m} = C_d A_g \sqrt{2\rho\Delta p}. \tag{86}$$

Let the six-apex candidate change gap area, pressure difference, and exposure time by:

$$A_{g,H} = \lambda_A A_{g,W}, \qquad \Delta p_H = \lambda_p \Delta p_W, \tag{87}$$

$$t_{open,H} = \lambda_t t_{open,W}. \tag{88}$$

The total leakage exposure scales approximately as:

$$M_{leak,H} \propto 6\lambda_A \sqrt{\lambda_p}\lambda_t. \tag{89}$$

For the triangular Wankel:

$$M_{leak,W} \propto 3. \tag{90}$$

For leakage not to worsen:

$$6\lambda_A \sqrt{\lambda_p}\lambda_t < 3, \tag{91}$$

hence:

$$\boxed{2\lambda_A \sqrt{\lambda_p}\lambda_t < 1.} \tag{92}$$

The parameter λ_t connects the leakage threshold with port and chamber timing. A shorter high-pressure exposure window can help satisfy Equation (92), but it may also reduce intake/exhaust duration and volumetric efficiency. The present model is apex-seal-only. Corner seals and side seals are not modelled here. For a six-apex rotor the number of corner interfaces also increases, and the full leakage model must treat apex, corner, and side seals separately, in the spirit of Picard et al. [8].

11.4 Wear threshold

Using Archard's wear relation:

$$V_{wear} = k\frac{F_s L}{H}, \tag{93}$$

where L is sliding distance and H is hardness. With six apexes, the total wear source count doubles. The six-apex design is advantageous only if the reduction in F_s and thermal instability is large enough to offset the increased number of sliding interfaces.

12 Six-Chamber Gas Exchange

Gas exchange must be evaluated because the six-chamber geometry may shorten the intake and exhaust windows. Define:

$$\Delta\theta_{int,i} = \theta_{IC,i} - \theta_{IO,i}, \tag{94}$$

$$\Delta\theta_{exh,i} = \theta_{EC,i} - \theta_{EO,i}. \tag{95}$$

The volumetric efficiency is:

$$\eta_v = \frac{m_{air,actual}}{\rho_{air} V_d}. \tag{96}$$

As a conservative first-order estimate, if six chamber events replace three chamber events over an equivalent rotor sequence and the port arc is not enlarged, then:

$$\Delta\theta_{int,H} \sim \frac{1}{2}\Delta\theta_{int,W}. \tag{97}$$

This is only a worst-case estimate, not final port timing. It assumes linear scaling with chamber count; the actual port duration depends on the five-lobe envelope, chamber trajectory, port geometry, and shaft-speed mapping. Equation (97) is important because it can work in opposite directions:

$$\lambda_t < 1 \quad \text{helps reduce leakage exposure,} \tag{98}$$

$$\eta_{v,H} < \eta_{v,W} \quad \text{hurts breathing and power.} \tag{99}$$

Therefore the design constraint is:

$$\eta_{v,H} \geq \eta_{v,W} - \epsilon_v, \tag{100}$$

with ϵ_v small enough that the torque and efficiency gains are not lost through poor breathing.

13 Efficiency as a Threshold Condition

For a spark-ignition engine, the ideal Otto efficiency is commonly written as:

$$\eta_{otto} = 1 - \frac{1}{r^{\gamma-1}}, \tag{101}$$

where r is compression ratio and γ is the heat-capacity ratio. This is only an upper-bound thermodynamic model; real brake thermal efficiency depends on combustion, heat transfer, leakage, friction, and pumping losses [3].

Let:

$$\eta_b = \eta_{otto}\Xi, \tag{102}$$

where:

$$\Xi = M_c M_h M_l M_f M_p. \tag{103}$$

Here M_c represents combustion completeness, M_h wall heat-transfer loss, M_l leakage, M_f mechanical friction, and M_p pumping loss. For $\gamma = 1.35$ and $r = 9$:

$$\eta_{otto,9} = 1 - 9^{-0.35} \approx 0.5365. \tag{104}$$

If a triangular Wankel reference has $\eta_b \approx 0.339$, then:

$$\Xi_W = \frac{0.339}{0.5365} = 0.632. \tag{105}$$

For a *Hexa-Wankel* candidate at $r = 10.5$:

$$\eta_{otto,10.5} = 1 - 10.5^{-0.35} \approx 0.561. \tag{106}$$

To exceed the triangular Wankel reference:

$$0.561\Xi_H > 0.339, \tag{107}$$

therefore:

$$\boxed{\Xi_H > 0.604.} \tag{108}$$

To reach a modern piston benchmark of approximately 40% BTE:

$$0.561\Xi_H > 0.40, \tag{109}$$

hence:

$$\boxed{\Xi_H > 0.713.} \tag{110}$$

Thus the strongest defensible claim is: the *Hexa-Wankel* can outperform a modern piston engine only if thermal-pressure stabilisation and loss reduction raise Ξ_H above 0.713 at $r_H = 10.5$.

14 Comparison with Piston Engines at Equal Effective Displacement

Comparison with piston engines must not use raw nominal cc. In a rotary engine, displacement depends on chamber swept volume, the number of events per shaft revolution, and effective air throughput. In this paper, *effective displacement* means the air-fuel volume actually compressed and expanded to produce work, normalised against comparable work events. All comparisons

with piston engines must be read in this sense, not as an administrative equivalence between rotary and piston cc.

At equal effective displacement, the *Hexa-Wankel* may have a power-density advantage because:

1. it lacks a large reciprocating piston mass;
2. torque may become more continuous if the two phased pulses succeed;
3. eccentricity can be reduced for the same displacement;
4. packaging may be more compact than a multi-cylinder piston engine.

Efficiency, however, does not automatically improve. Modern piston engines have optimised combustion, cooling, friction, porting, and ring-pack design for more than a century. A fair comparison must therefore satisfy:

$$\eta_{b,H} > \eta_{b,P}. \tag{111}$$

For a modern piston engine with $\eta_{b,P} \approx 0.40$, the $r_H = 10.5$ candidate requires $\Xi_H > 0.713$. This is a demanding target. The strongest thesis is therefore not that the *Hexa-Wankel* is necessarily more efficient, but that it has a theoretical path for turning rotary power density into efficiency, provided that sealing and thermal mapping truly become as predictable as those of the piston system.

15 Prior Art and Location of Novelty

This paper does not claim that all its components are new. Wankel geometry, trochoidal housing, apex-seal studies, and multiple-apex sealing have been discussed in the literature [1, 2, 9, 10]. Rose and Yang, for example, show that wide/multiple apex-seal designs can incorporate seal profiles into the housing design process and may improve sealing [9]. Warren also discusses a multi-apex sealing grid as an approach that can provide multiple leakage barriers and reduce the likelihood of seal separation [10].

The conceptual novelty of the *Hexa-Wankel* lies in the following combination:

1. definition of a six-apex rotor in a five-lobe Wankel-like baseline housing;
2. effective-displacement scaling that permits reduced eccentricity at equal displacement;
3. two phased combustion zones with unchanged total fuel, $Q/2 + Q/2$;
4. use of Fourier harmonic cancellation to formulate thermal stabilisation;
5. formulation of seal friction and leakage as thresholds, not as optimistic assumed values;
6. an explicit aim: to bring the rotary engine closer to piston-like thermal-sealing predictability.

The claimed originality is therefore not “six-sided rotary” in a general sense, but a threshold-based architecture combining kinematic scaling, phased combustion, thermal-harmonic reduction, and seal predictability.

16 Validation Status and Further Programme

Steps 1-4 of the validation programme have now been carried out at a preliminary theoretical level. The kinematic CAD model constructs the six-apex rotor, the gear law (9), and the five-lobe housing as an envelope. The actual chamber-volume calculation produces $V_i(\theta)$, $V_d = 35.786\,\text{cc}$ per chamber in the $R = 60\,\text{mm}$, $e = 8\,\text{mm}$, $b = 80\,\text{mm}$ model, and an additional clearance requirement of $3.714\,\text{cc}$ for the target $r = 10.5$. The subsequent numerical differentiation of the corrected volume curves produces preliminary torque kernels $K_i(\theta_s)$ and identifies candidate positive-expansion windows in Z_R and Z_L. The idealised 0-D pressure model then gives positive indicated work under finite-duration heat release.

The technical status is therefore: *basic 2D geometry passes, chamber-volume computability passes, preliminary positive-K_i phase placement passes, and idealised indicated work passes; final engine performance does not yet pass.* The model has not shown brake-power advantage, BSFC advantage, BTE advantage, production sealing feasibility, or real gas-exchange performance. For the hypothesis to become a robust engineering theory, the further programme must proceed in the following order:

1. **Conjugate geometry**: replace the first-order flank model with a full rotor-housing conjugacy proof, checking apex contact, chamber closure, and absence of interference over the entire cycle.
2. **Combustion-pocket optimisation**: design the clearance volume as a physical pocket rather than a volume addition, avoiding excessive surface-to-volume ratio, quenching, and hydrocarbon loss.
3. **Refined pressure model**: add wall heat transfer, residual gas, finite-rate combustion, pumping work, and friction mean effective pressure so that indicated work can be separated from brake work.
4. **Mechanical phase optimisation**: determine $\Delta\phi^*$ from Equation (52) using the refined $K_i(\theta_s)$ and $p_i(\theta)$ traces, then test compatibility with the 180° thermal-balancing separation.
5. **3D CAD refinement**: optimise rotor flank, side housing, axial volume, cooling passages, and seal packaging at a realistic scale.
6. **Port timing and gas exchange**: compute $\Delta\theta_{int}$, $\Delta\theta_{exh}$, overlap, η_v, mass-flow capability, and pumping work W_p in the actual five-lobe housing.
7. **CFD combustion**: test flame travel, turbulence, wall heat transfer, incomplete combustion, pressure trace, and the effect of the combustion pocket on quenching and hydrocarbon loss.
8. **FEA housing**: calculate thermal distortion, thermal stress, and σ_T^2 to ensure that thermal stabilisation is not merely a feature of the ideal Fourier model.
9. **Seal tribology and leakage**: model apex, corner, and side seals separately; measure F_s, lift-off, leakage area, friction, oil film, and wear.
10. **Scaling and dynamometer test**: repeat the calculation at 650–1300 cc effective displacement, then measure BSFC and BTE on a physical prototype or experimental rig.

With this status, the paper has passed initial geometric validation, preliminary torque-kernel phase validation, and idealised indicated-work validation. Efficiency claims must remain threshold-theoretic until gas exchange, heat loss, friction, CFD, FEA, tribology, and dynamometer tests are completed.

17 Falsification Conditions

The *Hexa-Wankel* hypothesis fails, or must be substantially revised, if any of the following conditions occurs:

1. the six-apex/five-lobe housing forms a cusp, self-intersection, or unsealable chamber;
2. the actual chamber volume does not permit $r \geq 10$ without a large dead volume;
3. the torque kernel does not provide two adequate positive expansion windows, or processes 2 and 5 cannot be placed in them;
4. the two-zone combustion separation $\theta_L = \theta_R + \pi$ is incompatible with $\Delta\phi^*$;
5. port timing causes a significant loss of volumetric efficiency;
6. $\lambda_F \lambda_v \geq 0.5$, so seal friction does not improve;
7. $2\lambda_A \sqrt{\lambda_p} \lambda_t \geq 1$, so leakage does not improve;
8. thermal variance $\sigma_{T,H}$ is not lower than that of the triangular Wankel;
9. scaling to 650–1300 cc effective displacement produces a surface-to-volume ratio, seal force, or thermal deformation that removes the design advantage;
10. simulated and dynamometer BTE do not exceed the Wankel comparator.

18 Conclusion

The *Hexa-Wankel* is a six-apex rotary-engine design hypothesis that attempts to combine Wankel power density with piston-like thermal-sealing predictability. The baseline design is a six-apex rotor in a five-lobe Wankel-like housing, with gear law $\psi = -\theta_s/6$. Two phased combustion points divide one fuel dose into two pulses, $Q/2 + Q/2$, rather than doubling the fuel.

The geometric analysis shows that the first-order envelope family has the regularity condition $R > ne$. Displacement scaling shows that the six-apex candidate has $V_{d,6}/V_{d,3} = 2$ at the same R, e, and b; therefore, at equal effective displacement, the six-apex design can reduce eccentricity or width. This provides a basis for the reduced-sliding-severity hypothesis, but it is not proof of efficiency.

The initial geometric contribution is no longer merely symbolic, but includes a two-dimensional kinematic CAD validation. At the baseline $R = 60\,\text{mm}$, $e = 8\,\text{mm}$, and $b = 80\,\text{mm}$, the actual chamber can be calculated with $V_d = 35.786\,\text{cc}$ per chamber. The raw model gives a near-zero V_{min}, showing that a real design must include a combustion pocket or clearance volume. With an additional clearance of $3.714\,\text{cc}$, the target $r = 10.5$ can be represented in the initial model. A subsequent torque-kernel extraction shows that positive-expansion windows exist and that candidate right/left combustion placements can be assigned to such windows. This supports the kinematic plausibility of the sequential-cycle interpretation $1 \to 2 \to 3 + 4 \to 5 \to 6$.

The thermodynamic contribution is now also explicit, though still preliminary. An idealised zero-dimensional pressure model using the unsmoothed clearance-corrected volume curve gives $W_H = 120.05\,\text{J} > 0$ for the dual-pulse pair, with $p_{max} = 81.14\,\text{bar}$ and $IMEP = 20.23\,\text{bar}$ under no-wall-loss assumptions. A fair equivalent-displacement single-pulse control gives

essentially the same ideal work and pressure, so the present model does not show automatic ideal-efficiency superiority. What it does support is redistribution of the work pulse: the theoretical torque-ripple index falls from 4.02 in a concentrated single-pulse comparison to 2.74 in the dual-pulse phase model.

The principal thermal contribution is the Fourier harmonic analysis: two opposed combustion zones in housing coordinates cancel the odd harmonics of heat flux, so the thermal map may become more stable. This is directly relevant to sealing. The sealing problem is not assumed to disappear; rather, the *Hexa-Wankel* attempts to make thermal distortion, pressure loading, seal preload, oil film, and leakage clearance more periodic and more calculable. The leakage sensitivity calculation confirms that this is decisive: at $5\,\mu$m equivalent gap, the estimated leakage is about 4.50%, whereas at $20\,\mu$m it rises to about 17.99%.

Tribologically, six apexes are advantageous only if $\lambda_F \lambda_v < 0.5$ for friction and $2\lambda_A \sqrt{\lambda_p} \lambda_t < 1$ for leakage. In efficiency terms, a candidate with target $r = 10.5$ must satisfy $\Xi_H > 0.604$ to outperform the 33.9% Wankel reference and $\Xi_H > 0.713$ to approach a modern piston engine at approximately 40% BTE. The *Hexa-Wankel* is therefore a coherent and falsifiable concept with preliminary geometric, torque-kernel, and idealised indicated-work support. It is not yet a final performance theory until conjugate 3D geometry, port timing, wall heat transfer, friction, CFD, FEA, seal dynamics, and dynamometer data are verified.

References

[1] Drogosz, P. (2010). "Geometry of the Wankel Rotary Engine." *Journal of KONES Powertrain and Transport*, 17(3), 89–94. Available at: `https://kones.eu/ep/2010/vol17/no3/9.pdf`

[2] Yamamoto, K. (1981). *Rotary Engine*. Toyo Kogyo / Mazda Motor Corporation.

[3] Heywood, J. B. (2018). *Internal Combustion Engine Fundamentals*, 2nd ed. McGraw-Hill Education.

[4] Toyota Motor Corporation. (2018). "2.0-litre Dynamic Force Engine, a New 2.0-litre Direct-injection, Inline 4-cylinder Gasoline Engine." Available at: `https://global.toyota/en/mobility/tnga/powertrain2018/engine/`

[5] Peden, M., Turner, J. W. G., Bailey, C., and Simmie, J. M. (2018). "Comparison of 1-D Modelling Approaches for Wankel Engine Performance Simulation and Initial Study of the Direct Injection Limitations." SAE Technical Paper 2018-01-1452.

[6] Zhang, Y. et al. (2021). "Research overview of rotary engine apex seals." *Chinese Journal of Engineering*. Indexed by DOAJ. Available at: `https://doaj.org/article/a99151dc910448d08c7eeff374fc9e24`

[7] Uner, E. and Cihan, O. (2025). "Analysis of Apex Seal Dynamic Behavior in a Wankel Engine." *International Journal of Automotive Science and Technology*. Available at: `https://dergipark.org.tr/en/pub/ijastech/article/1637285`

[8] Picard, M., Tian, T., and Nishino, T. (2016). "Predicting Gas Leakage in the Rotary Engine - Part I: Apex and Corner Seals." *Journal of Engineering for Gas Turbines and Power*, 138(6), 062503.

[9] Rose, S. W. and Yang, D. C. H. (2014). "Wide and multiple apex seals for the rotary engine." *Mechanism and Machine Theory*, 74, 202–215.

[10] Warren, S. (2012). *New Rotary Engine Designs by Deviation Function Method*. PhD dissertation, University of California, Davis. Available at: `https://escholarship.org/content/qt2w12f40z/qt2w12f40z.pdf`